tvst

Article

Decellularizing the Porcine Optic Nerve Head: Toward a Model to Study the Mechanobiology of Glaucoma

Jr-Jiun Liou[1,*], Michelle D. Drewry[1,*], Ashlinn Sweeney[1], Bryan N. Brown[1,2], and Jonathan P. Vande Geest[1–4]

[1] Department of Bioengineering, Swanson School of Engineering, University of Pittsburgh, Pittsburgh, PA, USA
[2] McGowan Institute for Regenerative Medicine, University of Pittsburgh, Pittsburgh, PA, USA
[3] Department of Ophthalmology, School of Medicine, University of Pittsburgh, Pittsburgh, PA, USA
[4] Louis J. Fox Center for Vision Restoration, University of Pittsburgh, Pittsburgh, PA, USA

Correspondence: Jonathan P. Vande Geest, Center for Bioengineering and Biotechnology, Room 409, University of Pittsburgh, 300 Technology Drive, Pittsburgh, PA 15213, USA. e-mail: jpv20@pitt.edu

Received: September 10, 2019
Accepted: April 7, 2020
Published: July 13, 2020

Keywords: decellularization; mechanobiology; glaucoma; lamina cribrosa; porcine

Citation: Liou J-J, Drewry MD, Sweeney A, Brown BN, Vande Geest JP. Decellularizing the porcine optic nerve head: toward a model to study the mechanobiology of glaucoma. Trans Vis Sci Tech. 2020;9(8):17, https://doi.org/10.1167/tvst.9.8.17

Purpose: Studying the extracellular matrix (ECM) remodeling of the lamina cribrosa in vivo can be extremely challenging and costly. There exist very few options for studying optic nerve head (ONH) mechanobiology in vitro that are able to reproduce the complex anatomic and biomechanical environment of the ONH. Herein, we have developed a decellularization procedure that will enable more anatomically relevant and cost-efficient future studies of ECM remodeling of the ONH.

Methods: Porcine posterior poles were decellularized using a detergent and enzyme-based decellularization protocol. DNA quantification and histology were used to investigate the effectiveness of the protocol. We subsequently investigated the ability of a polyethylene glycol (PEG)-based hydrogel to restore the ONH's ability to hold pressure following decellularization. Anterior-posterior displacement of the decellularized and PEG treated ONH in a pressure bioreactor was used to evaluate the biomechanical response of the ONH.

Results: DNA quantification and histology confirmed decellularization using Triton X-100 at low concentration for 48 hours successfully reduced the cellular content of the tissue by 94.9% compared with native tissue while preserving the ECM microstructure and basal lamina of the matrix. Infiltrating the decellularized tissues with PEG 6000 and PEG 10,000 hydrogel restored their ability to hold pressure, producing displacements similar to those measured for the non-decellularized control samples.

Conclusions: Our decellularized ONH model is capable of producing scaffolds that are cell-free and maintain the native ECM microstructure.

Translational Relevance: This model represents a platform to study the mechanobiology in the ONH and potentially for glaucoma drug testing.

Introduction

Glaucoma is a heterogeneous disorder characterized by progressive loss of retinal ganglion cells (RGCs) and is expected to affect 111.8 million people by the year 2040.[1] Currently, the only modifiable risk factor is elevated intraocular pressure (IOP).[2,3] Although many patients with glaucoma present with this increase in pressure, the disorder also occurs in patients with normal pressures, described as normal tension glaucoma.[4,5] In addition, patients can have elevated IOP, termed ocular hypertension, without developing retinal damage.[6,7] Together, these observations support the hypothesis that factors other than IOP play a role in glaucoma pathogenesis.

To further investigate the mechanisms behind glaucoma pathogenesis and progression, better model systems need to be developed, especially models of the optic nerve head (ONH) and lamina cribrosa (LC), the mesh-like tissue located in the ONH in which glaucomatous RGC degeneration is thought to originate. Although in vivo animal models offer many advantages, such models are also subject to a number of

limitations.[8] For example, rodents lack the collagenous extracellular matrix (ECM) present in the human LC, thus limiting their use in studying LC ECM remodeling.[8–10] Although large animals have an LC composed of a collagenous ECM, these models are expensive, low throughput, and lack the ability to be genetically and/or mechanically manipulated in a cost- and time-efficient manner, making mechanistic studies of LC ECM remodeling challenging.

As for in vitro models, two-dimensional cultures are unable to adequately represent the complex physiological ECM microstructure of the ONH and could lead to cell phenotypes that are unrepresentative of the in vivo state. Alternatively, explanted postmortem cadaver eyes offer an enticing alternative as they allow for a more accurate representation of the physiological environment of the eye. Use of cadaver eyes, however, results in native cell death within 72 hours following enucleation and thereby limits the time frame in which these tissues are viable for mechanobiological investigation. To bypass this postmortem degradation, tissues can be decellularized and used as a physiologically relevant scaffold for future cell seeding and culture.

Decellularization can be performed using chemical, physical, or enzymatic means to remove the cellular components from a tissue while maintaining its ECM microstructure. Decellularized tissues have been used as scaffolds, either with the structure intact or digested and formed into a hydrogel or film, for regeneration in a number of tissues, including the heart, peripheral nerves, and cornea, among numerous others.[11–14] Because tissues differ in their cellular and ECM composition and density, decellularization protocols needed to be tailored to each specific tissue of interest. Within the ocular field, studies have established decellularization protocols for the cornea, trabecular meshwork, retina, and optic nerve, although, in many of these studies, the decellularized tissues were subsequently homogenized and used to make a hydrogel.[13,15–17] To the best of our knowledge, no previous studies have attempted to decellularize the ONH or the LC for use as a biomimetic scaffold.

The purpose of this work is, therefore, to develop a method to decellularize porcine ONHs that removes cellular and genetic material and maintains the basement lamina and ECM microstructure of the tissue. Because biomechanical studies of the ONH require exposure to elevated IOP as is present in glaucoma, we investigated the use of a polyethylene glycol (PEG)-based hydrogel to recover the ability of the ONH to hold pressure following decellularization. The final decellularized and hydrogel-infiltrated tissue can then be used in cell culture as a more physiologically realistic scaffold. Overall, our platform can be used in the future to study the cellular mechanisms that contribute to glaucoma pathogenesis and progression, specifically those arising from dysregulation of the LC ECM.

Methods

Tissue Procurement and Dissection

Porcine eyes were purchased from Visiontech Inc. (Sunnyvale, TX), delivered within 24 hours postmortem, and stored on ice. Upon receipt, the eyes were dissected and hemisected to isolate the posterior pole. The choroid and retina were then removed and 1× phosphate buffered saline (PBS; Fisher Scientific, Hampton, NH) was used to keep the ocular tissues hydrated. Finally, the isolated posterior pole was cut into a clover leaf pattern, as shown in Figure 1A, and the optic nerve was trimmed to approximately 25 mm in length. Dissected posterior poles for decellularization were incubated in water overnight and then subjected to decellularization protocols, as described below; dissected posterior poles as control were immediately processed for DNA isolation or histology.

Decellularization

Our decellularization procedure was based on a protocol described by Prest et al. to decellularize canine sciatic nerves while maintaining the basal lamina.[18] This protocol was optimized for our porcine posterior poles by varying the concentration and duration of the Triton X-100 treatment and the concentration of the trypsin/ethylenediaminetetraacetic acid (EDTA) treatment (Table). Based on DNA quantification and histology results, we chose the lower concentration (0.1%) and longer duration (48 hours) of Triton X-100 treatment with 0.02%Trypsin/0.05% EDTA for 1 hour as our optimal protocol, which we then used for all subsequent experiments.

In the optimized protocol, posterior poles were incubated overnight in ultrapure Type I water (Milli-Q; MilliporeSigma, Burlington, MA) at 4°C. The next day, the tissues were treated with 0.02% trypsin (Fisher Scientific, Hampton, NH)/0.05% ethylenediaminetetraacetic acid (EDTA) (Fisher Scientific, Hampton, NH) at 37°C for 1 hour, followed by 48 hours of 0.1% Triton X-100 (Fisher Scientific), 15 minutes of 1M sucrose (Fisher Scientific), 1 hour of 4% deoxycholate (Sigma-Aldrich, St. Louis, MO), and 2 hours of 0.1% peracetic acid (Sigma-Aldrich) at room temperature. Tissues were shaken at 250 rpm for each incubation step and were washed with type I water until no foam

Table. Decellularization Protocols Evaluated in This Study

	Triton X-100		Trypsin/EDTA	
Group	Content	Duration	Content	Duration
High Triton, 1 h	3.0%	1 h	0.02% Trypsin/0.05% EDTA	1 h
Low Triton, 1 h	0.1%	1 h	0.02% Trypsin/0.05% EDTA	1 h
Low Triton, 48 h	0.1%	48 h	0.02% Trypsin/0.05% EDTA	1 h
Low Triton, 1 wk	0.1%	1 wk	0.02% Trypsin/0.05% EDTA	1 h
No Trypsin	3.0%	1 h	0% Trypsin/0% EDTA	1 h
High Trypsin	3.0%	1 h	0.1% Trypsin/0.25% EDTA	1 h

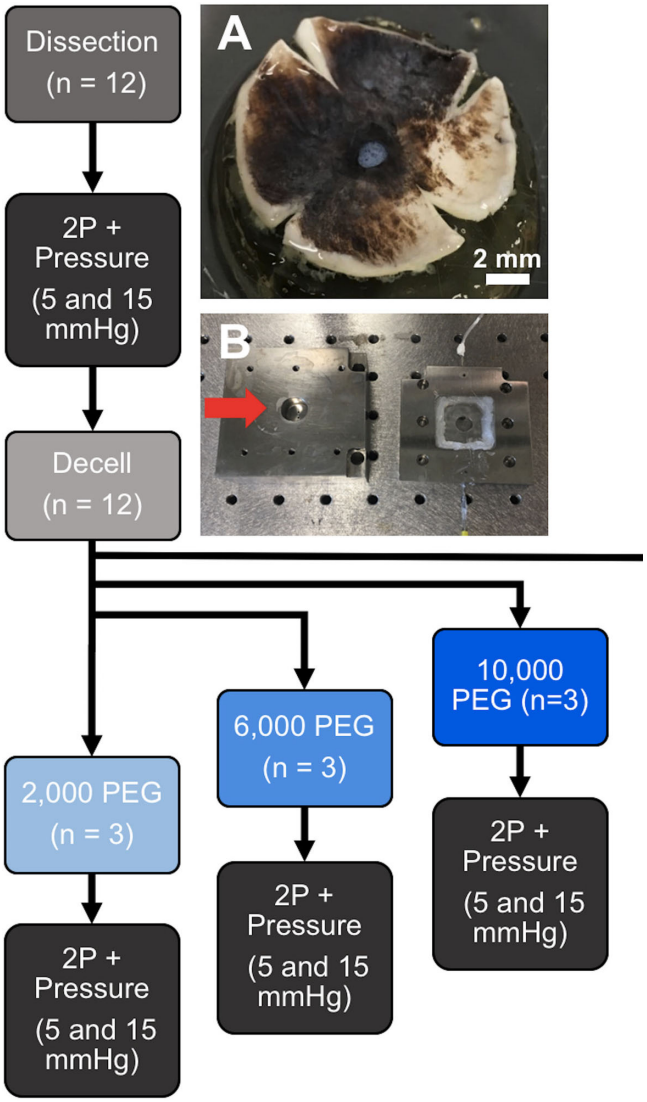

Figure 1. Design of pressurization and LC displacement experiment. Dissected porcine posterior poles were cut into a cloverleaf pattern (**A**) and positioned into a specialized pressurization chamber (**B**), designed to allow for visualizing the LC using two-photon microscopy while controlling the pressure upon the tissue. The overall experimental design is illustrated in the flow chart. Scale bar = 2 mm.

was observed at room temperature between each treatment. After the final treatment, the posterior poles were washed in type I water and then incubated in 1× PBS (Fisher Scientific) overnight at 4°C.

DNA Isolation and Characterization

Prior to DNA isolation, the posterior poles were frozen and lyophilized overnight, after which the dry weight of the tissue was recorded. The tissues were then digested overnight at 50°C using a proteinase K buffer (Invitrogen, Carlsbad, CA). Total DNA was isolated using phenol/chloroform/isoamyl alcohol (Sigma-Aldrich) and 3M sodium acetate (Sigma-Aldrich). Isolated DNA was reconstituted in TE buffer provided in the Quant-iT PicoGreen dsDNA Assay Kit (Invitrogen). This kit was then used to measure DNA concentration of the tissues according to the manufacturer's instructions.

Gel electrophoresis was performed to evaluate the quality of the DNA after decellularization, based on the size of the DNA fragments. Two percent (w/v) agarose I (Thermo Fisher, Pittsburgh, PA) in TAE buffer (Thermo Fisher) with 10,000X GelRed stock solution (Thermo Fisher) was used to make the agarose gel. For each sample, 1 ng/µl of DNA with 1:10 DNA Gel Loading Dye (Thermo Fisher) was loaded per well, and a Low DNA Mass Ladder (Thermo Fisher) was used to gauge the DNA degradation.

Histology

Tissues for histological analysis were fixed with 10% formalin, dehydrated in serial ethanol, and embedded in paraffin. Histological sections (10 µm) were stained with hematoxylin (Sigma-Aldrich) and eosin (Sigma-Aldrich) to evaluate the tissue structure and presence of nuclei. Immunostaining of collagen type IV and laminin was performed to evaluate the presence of

basal lamina proteins. Briefly, deparaffinized sections were blocked with bovine serum albumin (Fisher Scientific) and incubated in rabbit anti-collagen type IV (Abcam, Cambridge, UK; catalog #ab6586; concentration 1:1000) or rabbit anti-laminin (Abcam; catalog #ab11575; concentration 1:1000) at 4°C overnight, and then with goat anti-rabbit AF647 (Invitrogen; catalog #A-21244; concentration 1:1000) secondary antibodies at room temperature for 1 hour prior to addition of Fluoroshield Mounting Medium with DAPI (Abcam; catalog #ab104139).

Hydrogel Fabrication

The recipe for the poly(ethylene glycol) diacrylate (PEG-DA)/N-isopropylacrylamide (NIPAAm) hydrogel was adapted from that of Turturro et al.[19] In summary, 8 mM of PEG-DA (Sigma-Aldrich) was diluted in 1× PBS, using a PEG with a number average molar mass (Mn) of 2000, 6000, or 10,000 (with hydrogels using these PEGs subsequently referred to as PEG 2000, PEG 6000, and PEG 10,000). Poly(ethylene glycol)-block-poly NIPAAm (Sigma-Aldrich) was then used to make a 0.3 M PEG-DA/NIPAAm solution. The hydrogel was chemically cross-linked using 13 mM ammonium persulfate (Sigma-Aldrich) and 168 mM N,N,N′,N′-Tetramethylethylenediamine (TEMED; Sigma-Aldrich). When infiltrating the decellularized posterior poles with the hydrogel, the second crosslinker (TEMED) was not added until after the tissue was submerged in the hydrogel solution. After addition of TEMED, the tissue was gently swirled in the solution until the hydrogel formed.

Rheology

As a surrogate for stiffness, the storage moduli of the different PEG hydrogels were measured using the TA Instruments AR2000EX Rheometer (TA Instruments, New Castle, DE). The temperature was set to the desired start temperature, and the gap was set to 500 µm. A hydrogel solution without TEMED (0.8–1.0 mL) was prepared and stored on ice until the rheometer was ready. Once ready, the shields were removed, and the gap was set to 1200 µm. TEMED was added to the hydrogel solution immediately before loading the hydrogel onto the center of the platform. The gap was then set to 525 µm, and the geometry (40 mm parallel plate, Peltier Plate Steel) was placed in contact with the hydrogel. Finally, the shield was closed, and the gap was set to 500 µm for measurements with 5% strain at 1 Hz for a total of 600 seconds at a temperature of 37°C.

Pressurization and LC Displacement

We first assessed the ability of decellularized ONHs to hold pressure by determining if they were able to hold 45 mm Hg. This level of pressure was chosen as a conservative value in order to ensure our procedures would be able to hold any pressure from 5 to 45 mm Hg. Flattened tissues were clamped inside a customized pressurization chamber (see Fig. 1) connecting to a pressure transducer and a syringe filled with 1X PBS. When the pressure was set 45 mm Hg, the pressure curve went from baseline and stayed at 45 mm Hg if the sample was able to hold pressure; if not, the sample was labeled as incapable of holding pressure in the proportion results. The proportions were calculated using binary values indicating that the tissue was either capable (1) or incapable (0) of holding pressure.

To record the LC displacement, tissues were subjected to 5 and 15 mm Hg of pressure. Flattened tissues were clamped inside a customized pressurization chamber connecting to a pressure transducer and a syringe filled with 1X PBS. Three-dimensional (3D) images from an anterior viewpoint were taken using two-photon microscopy at 5 mm Hg and again at 15 mm Hg.[20,21] These pressures were chosen because the normal pressure in control pig eyes is reported 15.2 ± 2.1 mm Hg[22] and the LC showed the greatest displacement at these pressures in our previous study.[20,21,23] With this setup, we imaged the microstructural organization and mechanical response of the LC using an excitation wavelength of 780 nm, collecting collagen (collection 377/50 nm) and elastin (collection 460/80 nm) simultaneously. Image datasets from sequential levels of pressure at 5 and 15 mm Hg were de-noised, processed to measure anterior-posterior displacement of the LC, and normalized to the displacement of the same eye before decellularization. Decellularized tissues were unable to hold pressure, so we investigated the ability of hydrogel-infiltration and super glue coating to restore the biomechanical properties of the LC. This was accomplished by evaluating the tissues before decellularization and then after decellularization and treatment with either one of the PEG-based hydrogels (PEG 2000, PEG 6000, or PEG 10,000) or with super glue (Loctite, Westlake, OH). For the super glue treatment, the decellularized tissues were infiltrated with the PEG 10,000 hydrogel, then optic nerves were coated in super glue and allowed to completely dry before conducting pressurization experiments. For each ONH, displacement was measured both before (dissect) and after decellularization and treatment (decell). Displacement data was normalized to the displacement of the same sample prior to

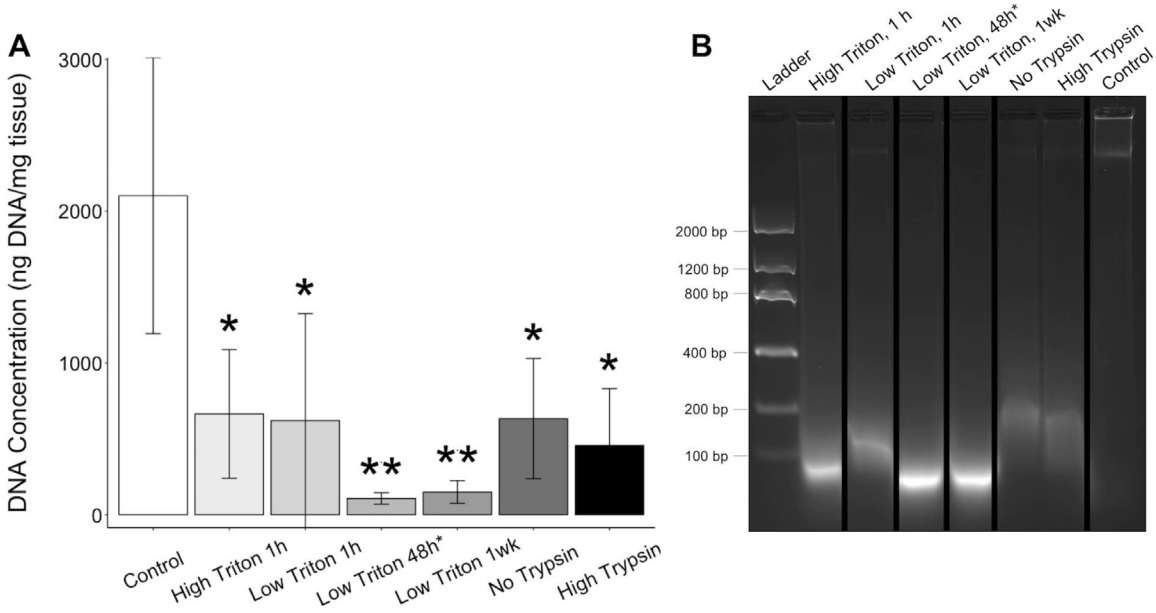

Figure 2. DNA content of the decellularized posterior poles compared to non-decellularized controls. To evaluate the ability of the decellularization protocol to remove cellular content, the DNA concentration was measured for both the decellularized posterior poles and their non-decellularized control (**A**), finding a significant decrease in the DNA concentration with decellularization for all protocols. Gel electrophoresis indicated that any remaining DNA in the decellularized tissues was more fragmented than in the controls (**B**). All samples were included in the same gel but not positioned adjacent, so cropping of the gel is indicated by black bars. *$P \leq 0.05$, **$P \leq 0.01$.

decellularization (non-decellularized controls) to control for between-sample variation.

Statistics

All experiments were conducted in triplicate (n-value = 3), and values are shown as the mean ± SD. Statistical differences were analyzed by (i) one-way ANOVA and Tukey's multiple comparisons and (ii) one-sample paired *t*-test for the anterior-posterior displacement of LC using the R statistical language and environment (R Foundation for Statistical Computing, Vienna, Austria), with significance at $P < 0.05$.[24]

Results

Decellularization Protocol Optimization

To develop a biomimetic scaffold of the ONH, we decellularized porcine posterior poles using a method optimized to preserve the ECM and structure of the tissue. We optimized this protocol for our tissues by modifying the concentration and duration of Triton X-100 treatment and the concentration of trypsin/EDTA treatment. Among six experimental groups - High Triton 1 h, Low Triton 1 h, Low Triton 48 h, Low Triton 1 wk, No Trypsin, and High Trypsin - we found a 68.4%, 70.5%, 94.9%, 92.9%, 69.9%, and 78.3% decrease in cellular DNA content compared with the control, with *P* values of 0.04, 0.03, 0.002, 0.004, 0.02, and 0.01, respectively (Fig. 2A). Although all modifications to the protocol were capable of significantly removing the cellular material from the tissues compared with the non-decellularized control and were not significantly different than original protocol[18], a longer duration (48 hours or 1 week) Triton X-100 treatment reduced the DNA content more than any other modification. The DNA from the extended Triton X-100 treatment protocols also appeared more degraded than those from the other protocols (Fig. 2B).

Histology was performed to further evaluate the ability of the decellularization protocols to remove cellular material and preserve the tissue structure. Hematoxylin and eosin (H&E) staining of the decellularized tissues confirmed that the protocols were successful in removing cellular material, as indicated by the minimal appearance of cell nuclei in the decellularized tissues compared with the non-decellularized controls (Fig. 3). The decellularization process did not appear to remove the pigment in the choroid. DAPI staining further validated these results, with less nuclei staining in the decellularized samples, especially those with longer duration Triton X-100 treatments

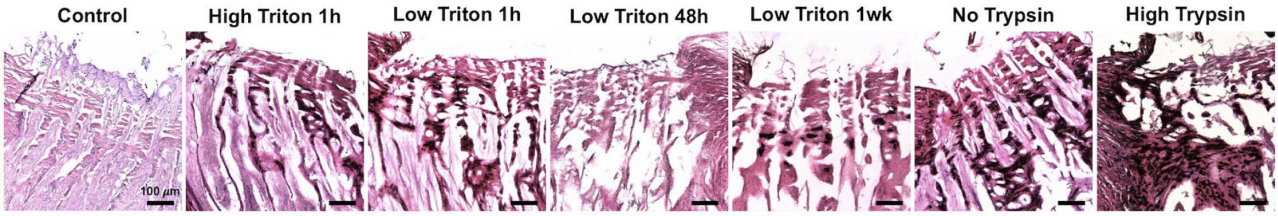

Figure 3. H&E staining of the decellularized posterior poles and non-decellularized controls. H&E staining was performed for the control and decellularization protocols with high triton for 1 hour, low triton for 1 hour, low triton for 48 hours, low triton for 1 week, no trypsin, and high trypsin. The resulting images indicate that remaining cellular content was negligible for all decellularization protocols, compared to the control, and that the different protocols preserved the ECM microstructure to varying degrees. Scale bar = 100 μm.

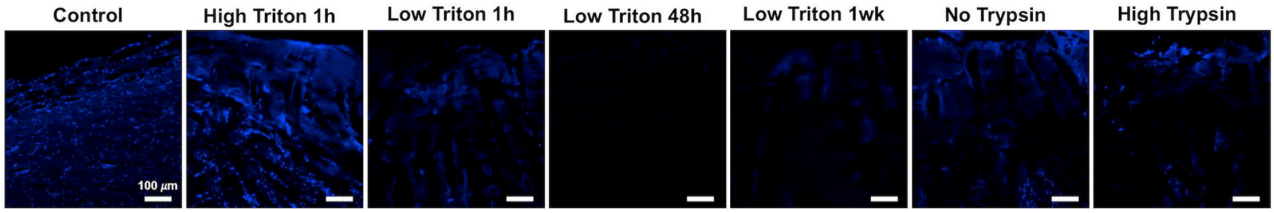

Figure 4. DAPI staining of the decellularized posterior poles and non-decellularized controls. DAPI staining was performed for the control and decellularization protocols with high triton for 1 hour, low triton for 1 hour, low triton for 48 hours, low triton for 1 week, no trypsin, and high trypsin. The resulting images confirmed the DNA quantification results in that the long duration triton treatments better cleared the tissues of cellular material. Scale bar = 100 μm.

(Fig. 4), although background fluorescence was seen in samples with residual pigment. Staining with H&E also indicated that the different decellularization protocols affected the ECM microstructure of the tissues to a varying level. As seen in Figure 3, treatment with a higher concentration of trypsin/EDTA destroyed the structure the most, whereas all other treatments were less harsh and better at maintaining the tissue architecture.

After evaluating the different decellularization protocols, we decided to proceed with the protocol that used a lower concentration of Triton X-100 for a longer duration. Because the Triton X-100 treatments for 48 hours and 1 week produced similar results, we chose to use the 48-hour treatment, thus minimizing the time required for decellularization. Overall, this protocol showed a decrease in the amount of cellular material compared to the non-decellularized controls, as indicated in Figure 2, by a significant decrease in DNA concentration (94.9% decrease with a P value of 0.00241) and more degraded DNA and in Figures 3 and 4 by the appearance of negligible levels of cell nuclei. It also preserved the structure of the tissue, as indicated by H&E staining (see Fig. 3). Using two-photon microscopy, we performed second harmonic generation (SHG) imaging to visualize the fibrillar collagen in the porcine posterior poles before and after decellularization, as seen in Figure 5. This imaging further confirmed that the ECM microstructure was maintained with our optimal decellularization protocol. Immunofluorescence staining for collagen IV and laminin indicated that the basement membrane was preserved after decellularization, as shown in Figure 5 by similar staining between the control and decellularized samples.

Rheology

Because decellularization caused the porcine posterior poles unable to hold pressure, we investigated the capability of holding pressure post decellularization using PEG-DA/NIPAAm hydrogels composed of three molecular weights (PEG 2000, PEG 6000, and PEG 10000). To confirm that increasing the molecular weight of the PEG would likewise increase the stiffness of the hydrogel, we performed rheology on all three hydrogels and measured their maximum storage modulus during the gelation process (Fig. 6). Results indicated that the PEG 6000 and PEG 10,000 hydrogels were significantly (P values of 0.000258 and 0.000140) stiffer than the PEG 2000 hydrogel, with storage moduli of 1.41 ± 0.797, 10.3 ± 1.60, and 11.3 ± 1.07 kPa, respectively. Although the PEG 10,000 hydrogel had a higher storage modulus than the PEG 6000 hydrogel, the difference was not significant, with a P value of 0.586.

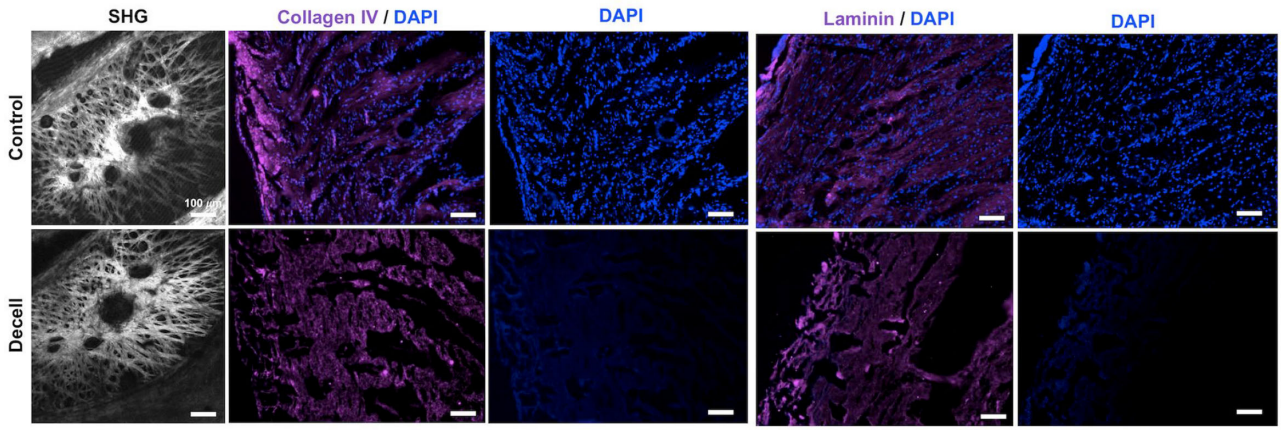

Figure 5. SHG and immunohistochemistry imaging of the decellularized posterior poles and non-decellularized controls. Histology was performed to compare the effect of decellularization on cellular content, ECM microstructure, and basal lamina of the tissue. SHG imaging of the control and decellularized posterior poles indicated that decellularization had minimal impact on ECM microstructure. DAPI (*blue*) staining validated the results from H&E staining, with the decellularized samples showing negligible cell nuclei compared to the controls. Tissues were stained for collagen IV (*magenta*) and laminin (*magenta*) to visualize the basal lamina, with similar immunofluorescence staining in the decellularized samples compared to the controls, indicating minimal damage to the basal lamina. Scale bar = 100 μm.

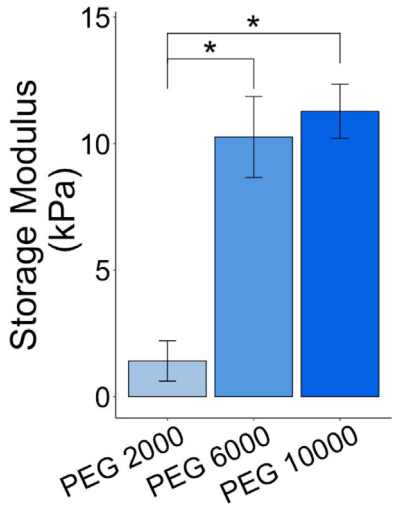

Figure 6. Storage moduli for the different PEG-DA/NIPAAm hydrogels. Rheology was used to compare the storage modulus of the three PEG-DA/NIPAAm hydrogels used in this study: PEG 2000, PEG 6000, and PEG 10,000. The storage modulus of the PEG 2000 hydrogel was found to be significantly lower than that of the PEG 6000 and PEG 10,000 hydrogels, with no significant difference between PEG 6000 and PEG 10,000 hydrogels. *$P \leq 0.05$.

Biomechanical Response of ONH Decellularization

The proportion of ONHs was calculated from the binary values indicating that the tissue was either capable (1) or incapable (0) of holding pressure of 45 mm Hg. Pressurizing the decellularized posterior poles confirmed that decellularization significantly reduces ability of the tissues to hold pressure, with 96.7% of the non-decellularized controls (Dissect) and among all the eyes tested, only 21.4% of the decellularized tissues (Decell) capable of holding pressure ($P < 0.001$; Fig. 7A). This is likely due to the removal of cellular material and neural tissues as a result of the decellularization process. Infiltrating the decellularized tissues with any of the PEG-based hydrogels restored their ability to hold pressure with no significant difference in success rate for the PEG 2000, PEG 6000, and PEG 10,000 compared with the non-decellularized controls (Dissect) (P values of 0.652, 0.581, and 0.525, respectively; see Fig. 7A).

After confirming that the PEG-based hydrogels were capable of holding pressure, we evaluated the biomechanical response of the hydrogel-infiltrated decellularized tissues. We utilized two-photon imaging to quantify the anterior to posterior displacement of the center of the LC in response to a pressure increase from 5 to 15 mm Hg. The ONHs of a set of decellularized posterior poles were coated with super glue, acting as positive control, because dried super glue is known to stiffen the tissue and, thus, reduce the displacement. After normalizing the measured displacement to the displacement prior to decellularization for the same eye (see Fig. 7B), we found that the PEG 2000-inflitrated tissues had a significantly greater displacement than before decellularization (P value of 8.60×10^{-5}) with all other groups remaining statistically similar ($P =$ 0.36, 0.96, and 0.12 for the PEG 6000, PEG 10,000, and glue groups, respectively). Therefore, the PEG 2000 hydrogel was unable to return the anterior to

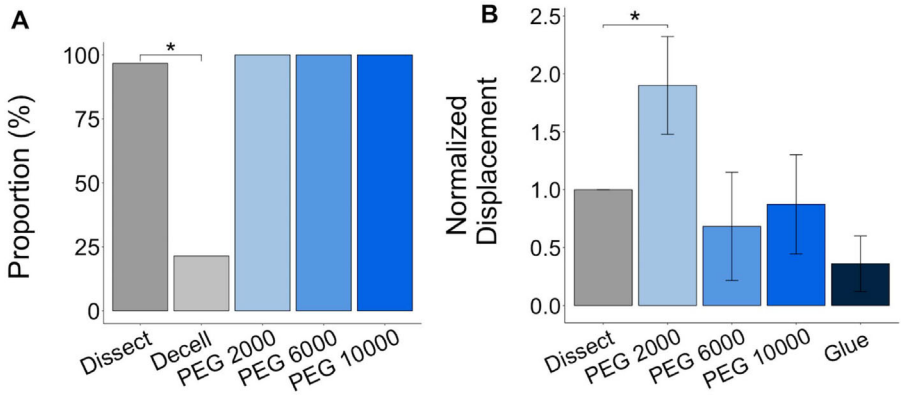

Figure 7. Pressurization of the posterior poles before and after decellularization and treatment with hydrogel or super-glue. Pressurizing the posterior poles to 15 mm Hg showed a significantly lower proportion (%) of the tissues were able to hold pressure after decellularization, but infiltrating the decellularized tissues with a PEG-based hydrogel enabled them to retain this ability (**A**). Measuring the displacement of the tissues after increasing the pressure on the tissues from 5 to 15 mm Hg showed that treating the decellularized tissues with either PEG 6000 or PEG 10,000 restored the biomechanical properties of tissue to that prior to decellularization (**B**). Dissect samples refers to the matched, non-decellularized controls, and displacement was normalized to the paired dissect displacement. *$P \leq 0.05$.

posterior displacement of the LC to its level prior to decellularization. Although there was no significant difference between the other treatment conditions, the PEG 6000 and PEG 10,000 hydrogel infiltration appeared to restore the biomechanical response of the decellularized ONH better than the glue-coating, having normalized displacements of 0.68 ± 0.5 and 0.87 ± 0.4, respectively, when the displacement of the non-decellularized controls (Dissect) was 1.00.

Discussion

Using an optimized decellularization protocol, we have developed a biomimetic scaffold that can be used to better study glaucoma and other diseases involved in ONH remodeling. The decellularization protocol was shown to remove cellular material while preserving the ECM microstructure and basal lamina in porcine posterior poles. Although the decellularized tissues could not hold pressure (which is needed for ONH mechanobiology investigations), we were able to restore the biomechanical response of the ONH by infiltrating it with a PEG-based hydrogel.

Decellularization is a process used to remove cellular material from tissues while preserving the ECM. Many techniques have been used to decellularize tissues, such as freeze-thaw cycles and treatment with detergents and other chemicals that disrupt the tissue and its cellular contents.[25] Because tissues vary in cellular and ECM composition, decellularization protocols need to be optimized for specific tissues. For our study, we chose to use a modification of a method described by Prest et al., designed to decellularize sciatic nerves with a series of detergents (sodium deoxycholate and Triton X-100), chemicals (EDTA and peracetic acid), and an enzyme (trypsin) interspersed by washes.[18]

Unlike ionic detergents, such as sodium dodecyl sulfate (SDS), Triton X-100 is less damaging to the structure of tissue.[26,27] Therefore, we manipulated the concentration and duration of Triton X-100 treatment when optimizing their protocol for the decellularization of porcine ONHs. As expected, increasing the duration of the treatment led to a greater removal of cellular material, as well as more damage to the ECM. To minimize damage, we chose to use a lower concentration of Triton X-100 when increasing the treatment duration, which led to removal of more cellular material while preserving the ECM microstructure. Increasing the concentration of Triton X-100 for the shorter treatment duration, though, also appeared to have negligible effects on the tissue microstructure, possibly because the concentration was still below the threshold of that capable of causing damage.

We also manipulated the concentration of trypsin/EDTA. Although EDTA is relatively ineffective alone, combining trypsin with EDTA enhances its ability to disrupt cell to ECM attachment, but trypsin has been found to also disrupt the ECM microstructure with prolonged treatment.[28,29] Thus, we only manipulated the concentration of the trypsin/EDTA treatment without increasing duration. We did not attempt to increase the duration or concentration of sodium deoxycholate or peracetic acid treatment, because they have been shown to cause aggregation

of DNA and increase ECM stiffness, respectively, and we wanted to minimize their harmful effects while still taking advantage of their ability to remove cellular material.[30–32]

In optimizing our decellularization protocol, a priority was maintaining the ECM of the ONH because the decellularized tissue is to be used to produce scaffolds to study the remodeling of the ONH in response to various levels of IOP. The ECM is composed of collagen, laminin, fibronectin, proteoglycans, and growth factors play an important role in cellular structure, signaling, and maintaining tissue-specific phenotypes.[33] The basement membrane of the ECM is important for anchoring certain cell populations.[34] Specific ECM and ultrastructural changes in the LC are associated with glaucoma, and remodeling of this tissue is a key clinical marker for this disease.[35] Yet, more studies are needed to better understand how ECM changes may contribute to glaucomatous damage, including retinal degradation and subsequent vision loss. Therefore, a scaffold that maintains the native ECM microstructure will be greatly beneficial to studying the glaucomatous ECM under physiologically relevant conditions.

Because the ONH is often pressurized in glaucoma biomechanical studies, we investigated the use of PEG-DA/NIPAAm hydrogels of varying molecular weight to restore the biomechanical response of the decellularized tissues. A PEG-DA/NIPAAm hydrogel was chosen because it has been previously used for intravitreal injections and is biocompatible with the retina.[19] The addition of PEG to the NIPAAm hydrogel adds to the mechanical strength of the hydrogel, with the molecular weight of the PEG directly proportional to the stiffness of the hydrogel.[36] Our results indicated that the higher molecular weight PEG evaluated (PEG 10,000) restored the biomechanical properties of the decellularized tissues more closely to that observed prior to decellularization, although there was no significant difference between the normalized displacements of the PEG 10,000 and PEG 6000 infiltrated tissues. If our scaffold is to be seeded with astrocytes and LC cells in future studies, it will need to be able to promote cell survival and astrocyte neurite outgrowth.

There are other biomechanical glaucoma models available for the characterization of LC microstructure. For example, Jan et al. also utilized microscopy to characterize collagen fiber organization without any immunolabeling.[37] This polarized light microscopy was able to capture high-resolution images providing information on fiber orientation.[37] In our study, we focus on capturing 3D images of collagen fibers in order to calculate the anterior-posterior displacement of the LC in response to IOP change. Another study described a methodology for building individual-specific computational models of ONH.[38] Using 3D, they reconstructed the anterior and posterior ONH surfaces from histological images providing information of Bruch's membrane opening, scleral curvature, and LC depth.[38] In our study, we were able to capture LC displacement without fixation, embedding, or sectioning of the tissues. When combined with the approach to quantify LC strain nondestructively that we described in our prior study, it will allow future investigations into the mechanobiology of ONH LC remodeling using human cells and human tissues.

One limitation of our study was the use of porcine posterior poles in lieu of postmortem human tissue. Although the porcine eye is a cost-efficient choice for preliminary studies, any differences in the ECM or cellular composition that do exist between species could change the effectiveness of the optimized decellularization protocol.[22] If a protocol similar to this is to be used in human tissues, the variation between species as well as human covariates including race, age, and gender may need to be taken into account both in optimizing the decellularization method and in the choice of hydrogel formulation used in mechanobiological studies. With the cellular material removed from the tissue, however, the decellularized posterior poles could likely be used for experiments utilizing recellularization and culture of human cells.[39] Future studies are needed to confirm that our decellularized scaffolds are indeed supportive of cell growth, allowing to establish a decellularization/recellularization platform to study the mechanobiology of glaucoma. Another limitation is that we focus on localized relative displacement rather than decomposing to tensile, compressive, or shear components. Most of the ONH biomechanical properties are measured using tensile tests, but it has been shown that the main mode of deformation under elevated intraocular pressure is compression.[40] Future studies will confirm whether the LC displacement measured in this study is a result of compression under elevated IOP from the anterior viewpoint.

In summary, we have successfully developed a physiologically relevant ONH scaffold using a mild decellularization protocol and a PEG-based hydrogel. Although previous studies have investigated decellularizing other ocular tissues, this is the first to optimize a decellularization protocol for the ONH. Our decellularization protocol was able to remove cellular material, preserve the ECM microstructure, and maintain the basal lamina. Infiltrating the tissues with a hydrogel can restore the ability of decellularized ONHs to hold pressure. Our decellularization model, therefore, can be used to establish an in vitro decellularization/recellularization platform to study the cellular

mechanisms involved in pathologies where LC ECM remodeling are prevalent, including primary open angle glaucoma.

Acknowledgments

The authors thank Travis Prest and Clint Skillen for their help with decellularization, lyophilization, and rheometry, as well as Daniela Krahe and Katelyn Axman for their help with the initial stages of the project.

Supported by the National Institutes of Health (NIH) R01EY020890 Grant to Jonathan P. Vande Geest, the NIH CORE Grant P30 EY08098 to the Department of Ophthalmology, the Eye and Ear Foundation of Pittsburgh, and an unrestricted grant from Research to Prevent Blindness, New York, NY. Additional support for this work is also provided by 1R01FD006582 (PI: Adam W. Feinberg, Co-I: Jonathan P. Vande Geest).

Disclosure: **J.-J. Liou,** None; **M.D. Drewry,** None; **A. Sweeney,** None; **B.N. Brown,** None; **J.P. Vande Geest,** None

* J-JL and MDD contributed equally to this study.

References

1. Tham Y-C, Li X, Wong TY, Quigley HA, Aung T, Cheng C-Y. Global prevalence of glaucoma and projections of glaucoma burden through 2040: a systematic review and meta-analysis. *Ophthalmology*. 2014;121:2081–2090.
2. Weinreb RN. IOP and the risk of progression to glaucoma. *Graefe's Archive for Clinical and Experimental Ophthalmology*. 2005;243:511–512.
3. Coleman AL, Miglior S. Risk factors for glaucoma onset and progression. *Survey of Ophthalmology*. 2008;53:S3–S10.
4. Li L, Bian A, Cheng G, Zhou Q. Posterior displacement of the lamina cribrosa in normal-tension and high-tension glaucoma. *Acta Ophthalmologica*. 2016;94:e492–e500.
5. Lee SH, Kim T-W, Lee EJ, Girard MJ, Mari JM, Ritch R. Ocular and clinical characteristics associated with the extent of posterior lamina cribrosa curve in normal tension glaucoma. *Scientific Reports*. 2018;8:961.
6. Kerr J, Nelson P, O'Brien C. A comparison of ocular blood flow in untreated primary open-angle glaucoma and ocular hypertension. *American Journal of Ophthalmology*. 1998;126:42–51.
7. Villarruel JM, Li XQ, Bach-Holm D, Hamann S. Anterior lamina cribrosa surface position in idiopathic intracranial hypertension and glaucoma. *European Journal of Ophthalmology*. 2017;27:55–61.
8. Bouhenni RA, Dunmire J, Sewell A, Edward DP. Animal models of glaucoma. *BioMed Research International*. 2012;2012:692609.
9. Almasieh M, Levin LA. Neuroprotection in glaucoma: animal models and clinical trials. *Annual Review of Vision Science*. 2017;3:91–120.
10. May CA. Comparative anatomy of the optic nerve head and inner retina in non-primate animal models used for glaucoma research. *The Open Ophthalmology Journal*. 2008;2:94.
11. Gilbert TW, Sellaro TL, Badylak SF. Decellularization of tissues and organs. *Biomaterials*. 2006;27:3675–3683.
12. Hudson TW, Liu SY, Schmidt CE. Engineering an improved acellular nerve graft via optimized chemical processing. *Tissue Engineering*. 2004;10:1346–1358.
13. Lynch AP, Ahearne M. Strategies for developing decellularized corneal scaffolds. *Experimental Eye Research*. 2013;108:42–47.
14. Ott HC, Matthiesen TS, Goh S-K, et al. Perfusion-decellularized matrix: using nature's platform to engineer a bioartificial heart. *Nature Medicine*. 2008;14:213.
15. Dang Y, Waxman S, Wang C, et al. Freeze-thaw decellularization of the trabecular meshwork in an ex vivo eye perfusion model. *PeerJ*. 2017;5:e3629.
16. Kundu J, Michaelson A, Talbot K, Baranov P, Young MJ, Carrier RL. Decellularized retinal matrix: natural platforms for human retinal progenitor cell culture. *Acta Biomaterialia*. 2016;31:61–70.
17. Crapo PM, Medberry CJ, Reing JE, et al. Biologic scaffolds composed of central nervous system extracellular matrix. *Biomaterials*. 2012;33:3539–3547.
18. Prest TA, Yeager E, LoPresti ST, et al. Nerve-specific, xenogeneic extracellular matrix hydrogel promotes recovery following peripheral nerve injury. *Journal of Biomedical Materials Research Part A*. 2018;106:450–459.
19. Turturro SB, Guthrie MJ, Appel AA, et al. The effects of cross-linked thermo-responsive PNIPAAm-based hydrogel injection on retinal function. *Biomaterials*. 2011;32:3620–3626.
20. Pyne JD, Genovese K, Casaletto L, Geest JPV. Sequential-digital image correlation for mapping

human posterior sclera and optic nerve head deformation. *Journal of Biomechanical Engineering*. 2014;136:021002.
21. Tamimi EA, Pyne JD, Muli DK, et al. Racioethnic differences in human posterior scleral and optic nerve stump deformation. *Investigative Ophthalmology & Visual Science*. 2017;58:4235–4246.
22. Ruiz-Ederra J, Garcia M, Hernandez M, et al. The pig eye as a novel model of glaucoma. *Exp Eye Res*. 2005;81:561–569.
23. Behkam R, Kollech HG, Jana A, et al. Racioethnic differences in the biomechanical response of the lamina cribrosa. *Acta Biomaterialia*. 2019;88:131–140.
24. Team RC. *R: A Language and Environment for Statistical Computing*. Vienna, Austria: R Foundation for Statistical Computing; 2019.
25. Crapo PM, Gilbert TW, Badylak SF. An overview of tissue and whole organ decellularization processes. *Biomaterials*. 2011;32:3233–3243.
26. Adair-Kirk TL, Senior RM. Fragments of extracellular matrix as mediators of inflammation. *The International Journal of Biochemistry & Cell Biology*. 2008;40:1101–1110.
27. Stern MM, Myers RL, Hammam N, et al. The influence of extracellular matrix derived from skeletal muscle tissue on the proliferation and differentiation of myogenic progenitor cells ex vivo. *Biomaterials*. 2009;30:2393–2399.
28. Sawada K, Terada D, Yamaoka T, Kitamura S, Fujisato T. Cell removal with supercritical carbon dioxide for acellular artificial tissue. *Journal of Chemical Technology & Biotechnology: International Research in Process, Environmental & Clean Technology*. 2008;83:943–949.
29. Gilpin A, Yang Y. Decellularization strategies for regenerative medicine: from processing techniques to applications. *BioMed Research International*. 2017;2017:9831534.
30. Gilbert TW, Gilbert S, Madden M, Reynolds SD, Badylak SF. Morphologic assessment of extracellular matrix scaffolds for patch tracheoplasty in a canine model. *The Annals of Thoracic Surgery*. 2008;86:967–974.
31. Meezan E, Hjelle JT, Brendel K, Carlson EC. A simple, versatile, nondisruptive method for the isolation of morphologically and chemically pure basement membranes from several tissues. *Life Sciences*. 1975;17:1721–1732.
32. Syed O, Walters NJ, Day RM, Kim H-W, Knowles JC. Evaluation of decellularization protocols for production of tubular small intestine submucosa scaffolds for use in oesophageal tissue engineering. *Acta Biomaterialia*. 2014;10:5043–5054.
33. Hynes RO. The extracellular matrix: not just pretty fibrils. *Science*. 2009;326:1216–1219.
34. Brown B, Lindberg K, Reing J, Stolz DB, Badylak SF. The basement membrane component of biologic scaffolds derived from extracellular matrix. *Tissue Engineering*. 2006;12:519–526.
35. Hernandez MR. The optic nerve head in glaucoma: role of astrocytes in tissue remodeling. *Progress in Retinal and Eye Research*. 2000;19:297–321.
36. Alexander A, Ajazuddin Khan J, Saraf S, Saraf S. Polyethylene glycol (PEG)-Poly(N-isopropylacrylamide) (PNIPAAm) based thermosensitive injectable hydrogels for biomedical applications. *European Journal of Pharmaceutics and Biopharmaceutics*. 2014;88:575–585.
37. Jan NJ, Grimm JL, Tran H, et al. Polarization microscopy for characterizing fiber orientation of ocular tissues. *Biomedical Optics Express*. 2015;6:4705–4718.
38. Schwaner SA, Kight AM, Perry RN, et al. A methodology for individual-specific modeling of rat optic nerve head biomechanics in glaucoma. *Journal of Biomechanical Enginering*. 2018;140:0845011.
39. Hutter H, Vogel BE, Plenefisch JD, et al. Conservation and novelty in the evolution of cell adhesion and extracellular matrix genes. *Science*. 2000;287:989–994.
40. Downs JC, Roberts MD, Burgoyne CF. Mechanical environment of the optic nerve head in glaucoma. *Optometry and Vision Science*. 2008;85:425–435.